

## THE STELLAR INITIAL MASS FUNCTION AT $0.9 < z < 1.5$

IGNACIO MARTÍN-NAVARRO<sup>1,2</sup>, PABLO G. PÉREZ-GONZÁLEZ<sup>3,4</sup>, IGNACIO TRUJILLO<sup>1,2</sup>, PILAR ESQUEJ<sup>3</sup>, ALEXANDRE VAZDEKIS<sup>1,2</sup>, HELENA DOMÍNGUEZ SÁNCHEZ<sup>3</sup>, GUILLERMO BARRO<sup>5</sup>, GUSTAVO BRUZUAL<sup>6</sup>, STÉPHANE CHARLOT<sup>7</sup>, ANTONIO CAVA<sup>8</sup>, IGNACIO FERRERAS<sup>9</sup>, NÉSTOR ESPINO<sup>3</sup>, FRANCESCO LA BARBERA<sup>10</sup>, ANTON M. KOEKEMOER<sup>11</sup>, A. JAVIER CENARRO<sup>12</sup>

<sup>1</sup>Instituto de Astrofísica de Canarias, c/ Vía Láctea s/n, E38205 - La Laguna, Tenerife, Spain

<sup>2</sup>Departamento de Astrofísica, Universidad de La Laguna, E-38205 La Laguna, Tenerife, Spain

<sup>3</sup>Departamento de Astrofísica, Facultad de CC. Físicas, Universidad Complutense de Madrid, E-28040 Madrid, Spain

<sup>4</sup>Severo Ochoa Visitor at Instituto de Astrofísica de Canarias

<sup>5</sup>UCO/Lick Observatory, Department of Astronomy and Astrophysics, University of California, Santa Cruz, CA 95064, USA

<sup>6</sup>Centro de Radioastronomía y Astrofísica, UNAM, Campus Morelia, México

<sup>7</sup>UPMC-CNRS, UMR7095, Institut d'Astrophysique de Paris, F-75014 Paris, France

<sup>8</sup>Observatoire de Genève, Université de Genève, 51 Ch. des Maillettes, 1290, Versoix, Switzerland

<sup>9</sup>Mullard Space Science Laboratory, University College London, Holmbury St Mary, Dorking, Surrey RH5 6NT

<sup>10</sup>INAF - Osservatorio Astronomico di Capodimonte, Napoli, Italy

<sup>11</sup>Space Telescope Science Institute, 3700 San Martin Drive, Baltimore, MD 21218, USA and

<sup>12</sup>Centro de Estudios de Física del Cosmos de Aragón, Plaza San Juan 1, 44001 Teruel, Spain

*Draft version November 25, 2014*

### ABSTRACT

We explore the stellar initial mass function (IMF) of a sample of 49 massive quiescent galaxies (MQGs) at  $0.9 < z < 1.5$ . We base our analysis on intermediate resolution spectro-photometric data in the GOODS-N field taken in the near-infrared and optical with the HST/WFC3 G141 grism and the Survey for High- $z$  Absorption Red and Dead Sources (SHARDS). To constrain the slope of the IMF, we have measured the TiO<sub>2</sub> spectral feature, whose strength depends strongly on the content of low-mass stars, as well as on stellar age. Using ultraviolet to near-infrared individual and stacked spectral energy distributions, we have independently estimated the stellar ages of our galaxies. Knowing the age of the stellar population, we interpret the strong differences in the TiO<sub>2</sub> feature as an IMF variation. In particular, for the heaviest  $z \sim 1$  MQGs ( $M > 10^{11} M_{\odot}$ ) we find an average age of  $1.7 \pm 0.3$  Gyr and a bottom-heavy IMF ( $\Gamma_b = 3.2 \pm 0.2$ ). Lighter MQGs ( $2 \times 10^{10} < M < 10^{11} M_{\odot}$ ) at the same redshift are younger on average ( $1.0 \pm 0.2$  Gyr) and present a shallower IMF slope ( $\Gamma_b = 2.7^{+0.3}_{-0.4}$ ). Our results are in good agreement with the findings about the IMF slope in early-type galaxies of similar mass in the present-day Universe. This suggests that the IMF, a key characteristic of the stellar populations in galaxies, is bottom-heavier for more massive galaxies and has remained unchanged in the last  $\sim 8$  Gyr.

*Subject headings:* galaxies: formation — galaxies: evolution — galaxies: high-redshift — galaxies: fundamental parameters — galaxies: stellar content

### 1. INTRODUCTION

The initial mass function (IMF) dictates the distribution of stellar masses for any single star formation event in a galaxy. Consequently, it determines the number of massive stars formed and being responsible for the feedback and chemical processes. The IMF also fix the numbers of low-mass stars, which dominate the total stellar mass of a galaxy.

Growing evidence support a non-universal IMF in the nearby Universe, where massive early-type galaxies (ETGs) show an enhanced fraction of dwarf stars in the center compared to the Milky Way (van Dokkum & Conroy 2010). Moreover, the dwarf-to-giant ratio, i.e., the IMF slope, correlates with the central velocity dispersion (Cenarro et al. 2003; Treu et al. 2010; Cappellari et al. 2012; Ferreras et al. 2013a; La Barbera et al. 2013; Conroy et al. 2013; Spiniello et al. 2014). These results challenge the existence of a universal IMF inferred from resolved stellar population analysis in the Local Group (Kroupa 2002; Bastian et al. 2010; Kroupa et al. 2013).

To have a consistent picture of galaxy evolution, it is absolutely necessary to investigate the IMF at different redshifts. So far, the IMF of  $z \lesssim 1$  galaxies has been studied indirectly using virial masses (Renzini 2006; van de Sande et al. 2013) or elaborated dynamical models (Shetty & Cappellari 2014). These works point to a Salpeter (1955) IMF for massive galaxies at intermediate redshift. Other indirect IMF-sensitive observables have also been used in the topic. For instance, the consistency between the cosmic stellar mass and star formation rate densities (Davé 2008; Pérez-González et al. 2008) and the luminosity evolution of massive ETGs (van Dokkum 2008) are better described by a flatter (i.e., with a relatively larger number of massive stars) IMF at higher look-back times. Even in star-forming galaxies, the constancy of the IMF is in tension with observations (Hoversten & Glazebrook 2008; Meurer et al. 2009).

Here we explore, for the first time, the IMF slope at  $z \gtrsim 1$  using stellar populations synthesis models in massive quiescent galaxies (MQGs). To achieve this goal, we study the TiO<sub>2</sub> IMF-sensitive spectral feature (Mould 1976). In Section 2, we describe the data. The IMF inference is explained in Section 3. In Section 4, we discuss

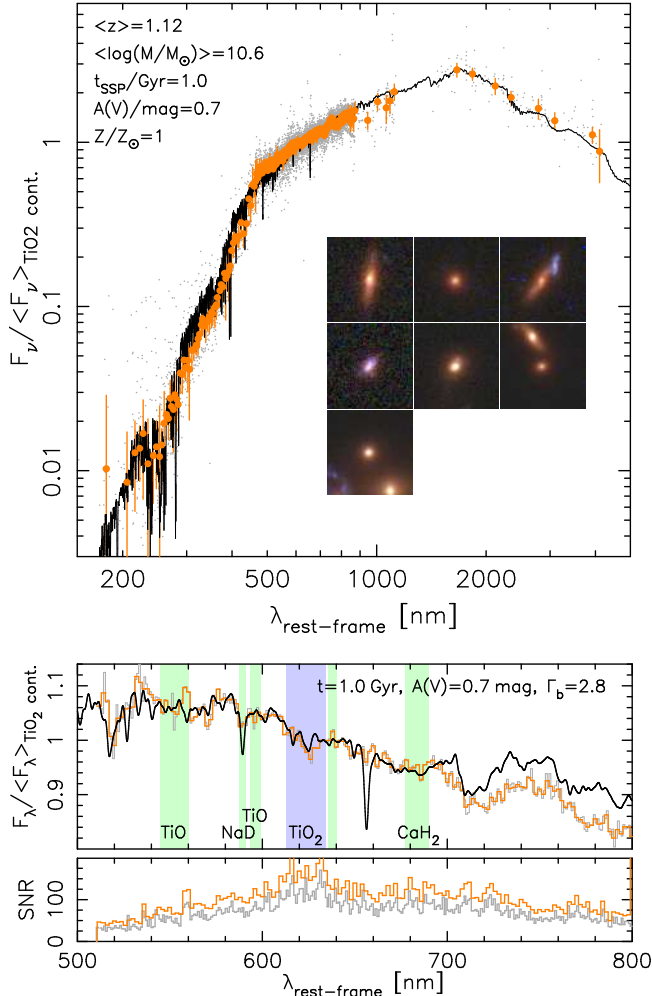


FIG. 1.— Stacked SEDs (normalized to the average  $\text{TiO}_2$  continuum flux) for MQGs at  $0.9 < z < 1.5$  in GOODS-N for the low-mass sample. We show the complete UV-to-NIR stack on *top*, with data for individual galaxies (gray dots) and average fluxes in bins of 20 photometric data points (orange), including  $2\sigma$  bars. The black line shows best-fitting SSP models (BC03/XMILES, Kroupa IMF, Calzetti et al. (2000) attenuation law). We provide  $5'' \times 5''$  RGB postage stamps for representative examples of the sample. At the *bottom*, we show the WFC3/G141 grism data including stacked (gray) and smoothed (orange) spectra (using 10 and 20 Å bins, respectively), and their SNR. The black line shows best-fitting MUSECAT SSP models. Shaded regions mark the  $\text{TiO}$  absorption (blue), and other IMF-sensitive indices (green). Deviations from an SSP appear beyond 700nm, where a small fraction ( $\sim 10\%$ ) of a younger population can significantly affect the continuum, but barely changes (0.004 mag) the  $\text{TiO}_2$  value.

our results. We adopt a standard cosmology:  $H_0 = 70 \text{ km s}^{-1} \text{ Mpc}^{-1}$ ,  $\Omega_m = 0.3$ , and  $\Omega_\Lambda = 0.7$ .

## 2. SAMPLE AND DATA DESCRIPTION

To facilitate the determination of the IMF slope at high- $z$ , we study galaxies with no signs of recent star formation (quiescent galaxies). These objects have simpler Star Formation Histories (SFHs) than star-forming galaxies and are sufficiently well represented by a single stellar population (SSP) model (e.g., Whitaker et al. 2013).

MQGs at  $0.9 < z < 1.5$  were selected with two criteria: (1) the  $UVJ$  diagram complemented with fluxes in the MIR/FIR; and (2) a sSFR vs. stellar mass

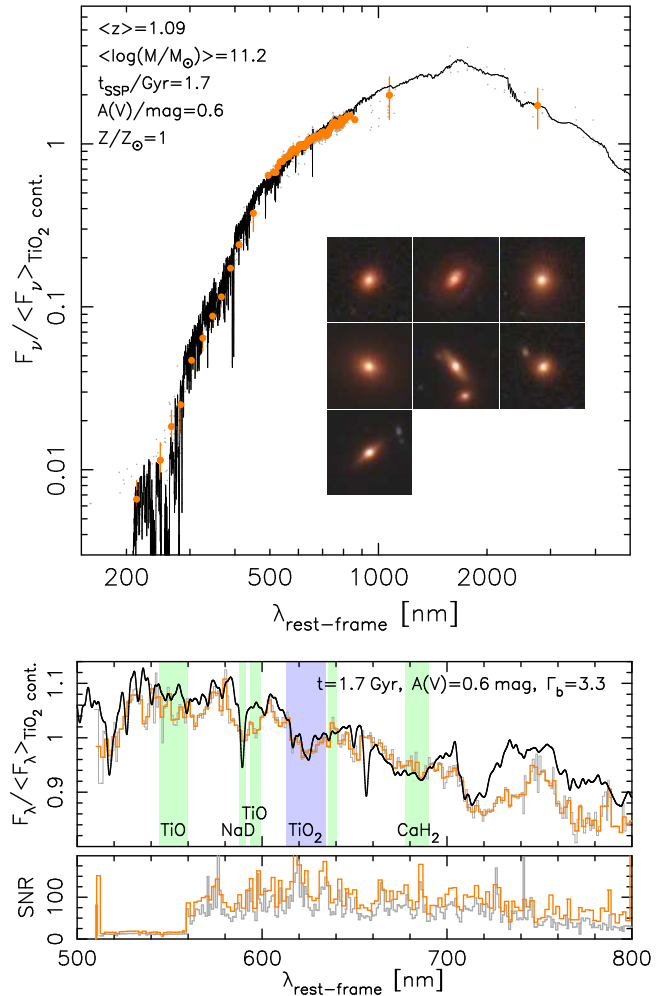


FIG. 2.— Same as Fig. 1 but for the high-mass sample.

plot. We worked with the mass selected sample presented in Pérez-González et al. (2008). From this work, we took the spectral energy distributions (SEDs), stellar population and dust emission models for all IRAC sources in GOODS-N. Those SEDs were complemented with medium-band optical photometry from the Survey for High- $z$  Absorption Red and Dead Sources, SHARDS (Pérez-González et al. 2013). The broad- and medium-band photometry was fitted with a variety of stellar population models to obtain photometric redshifts, stellar masses, SFRs, and rest-frame synthetic colors (see Barro et al. 2011a,b). Thanks to the ultra-deep medium-band data from SHARDS, the quality of our photometric redshifts is excellent: the median  $\Delta z / (1+z)$  is 0.0067 for the 2650 sources with  $I < 25$  (Pérez-González et al. 2014, in prep; Ferreras et al. 2013b). SFRs were calculated for all galaxies using various dust emission templates and the *Spitzer*-MIPS and *Herschel*-PACS/SPIRE fluxes, jointly with UV-based measurements for non-detections in the MIR/FIR. The UV-based SFRs were corrected for extinction with the UV slope  $\beta$  and an extrapolation of the IR- $\beta$  (IRX) relationship (Meurer et al. 1999). The extrapolation technique was developed to recalibrate the IRX- $\beta$  relation using faint IR emitters (more similar to MIR-undetected galaxies) at the same redshifts. Details

about the selection will be given in Domínguez Sánchez *et al.* (2014, in prep.).

Using this dataset, we selected galaxies at  $0.9 < z < 1.5$  having stellar masses  $M > 2 \times 10^{10} M_{\odot}$  (Kroupa 2001 IMF), and rest-frame  $UVJ$  colors within the quiescent galaxy wedge ( $U-V > 1.3$ ,  $V-J < 1.6$ ,  $U-V > 0.88 \times (V-J) + 0.59$ ; Whitaker *et al.* 2011). The mass cut was chosen to allow measuring the  $\text{TiO}_2$  absorption in the grism spectra described below. The  $UVJ$ -selected sample was complemented with galaxies with  $\text{sSFR} < 0.2 \text{ Gyr}^{-1}$ , our limit for quiescence. Galaxies with MIPS detections were removed from the sample, as the MIR emission indicates active/residual star formation or nuclear activity, which would complicate the stellar population analysis. Using these two criteria, we selected 124 sources in the  $112 \text{ arcmin}^2$  covered simultaneously by GOODS, SHARDS, CANDELS, and *Herschel*-GOODS.

The  $\text{TiO}_2$  spectral index was measured in stacked WFC3/G141 grism data (covering  $1.1 \lesssim \lambda \lesssim 1.6 \mu\text{m}$ ) from the AGHAST survey (PI: Weiner). We selected all galaxies with  $H < 25.5 \text{ mag}$  from the F160W imaging in CANDELS (Grogin *et al.* 2011; Koekemoer *et al.* 2011) and reduced the grism data to extract 2D spectra using the aXe software (version 2.3). Then we collapsed the data to obtain 1D spectra using our own dedicated software. The reduction used  $0.064 \text{ arcsec/pixel}$  and  $23.5 \text{ Å/pixel}$ . The 1D extractions were optimized for each galaxy using its effective radius, position angle, and the contamination map provided by aXe. Visual inspection helped to remove spectra with significant contamination and/or artifacts, leaving 97 galaxies with usable G141 spectra. We kept the spectra with  $\text{SNR} > 5$  per pixel. Our final sample is composed by 57 galaxies with  $2 \times 10^{10} < M/M_{\odot} < 10^{11.5}$  ( $\langle M \rangle = 10^{10.6} M_{\odot}$ ) and  $0.9 < z < 1.5$  ( $\langle z \rangle = 1.1$ ). Reliable spectroscopic redshifts were available for 33 galaxies; the median quality of the photo-redshifts for  $M > 10^{10.5} M_{\odot}$  galaxies is  $\Delta z / (1+z) = 0.0047$ .

Measurements were carried out in stacked spectra of these 57  $z \sim 1$  MQGs. We dissected the sample to probe the lowest and highest mass regimes with two stacked spectra of similar SNR (Figures 1,2). The high-mass sample was composed by 7 galaxies with  $M > 10^{11} M_{\odot}$  ( $H = 19.7\text{--}21.3 \text{ mag}$ ), and the low-mass spectra by 50 galaxies with  $M < 2 \times 10^{10} M_{\odot}$  ( $H = 20.3\text{--}22.4 \text{ mag}$ ). To build the stacks, we first de-redshifted all individual observed spectra, then normalizing them to the  $\text{TiO}_2$  continuum (see next section). We calculated flux averages and errors in rest-frame wavelength bins of  $10 \text{ Å}$ . Finally, we smoothed the stacks with a  $20 \text{ Å}$  boxcar kernel. The average SNR per resolution element of the final stacked (smoothed) spectra is 70 (100), 100 (140) around the  $\text{TiO}_2$  absorption.

### 3. SED ANALYSIS: AGES AND IMF SLOPE

The integrated spectral properties of a SSP are defined by four parameters: age, metallicity ( $[Z/H]$ ), IMF and  $\alpha$ -elements over-abundance ( $[\alpha/\text{Fe}]$ ). In this Letter, we analyze the  $\text{TiO}_2$  absorption, an IMF-sensitive feature which depends very weakly on  $[Z/H]$  and  $[\alpha/\text{Fe}]$  (Thomas *et al.* 2011; La Barbera *et al.* 2013). We present the age and IMF constraints for  $z \sim 1$  MQGs based on this  $\text{TiO}_2$  spectral index as well as on the ultra-

violet to near-infrared SEDs. In Section 4, we discuss the impact of the unknown values of  $[Z/H]$  and  $[\alpha/\text{Fe}]$  on our results. The  $\text{TiO}_2$  absorption is wide and deep enough to be measured with WFC3 grism data. Measurements for other IMF-sensitive features (see Figures 1,2) would be compromised by low SNR at  $\lambda_{\text{rf}} < 500 \text{ nm}$ , the low spectral resolution in the case of NaD, or the proximity to emission features in the case of  $\text{CaH}_2$ . Thus, we concentrate our IMF analysis on  $\text{TiO}_2$  measurements.

#### 3.1. Age determination

To constrain the age of the stellar population, we used three different methods. First, we fitted the G141 grism stacked spectra constrained to the rest-frame wavelength range  $500 < \lambda_{\text{rf}} < 800 \text{ nm}$  (Figures 1,2). We used the Bruzual & Charlot (2003, hereafter BC03) models fed with the XMMILES library (Charlot & Bruzual, private communication). We assumed a SSP with solar and super-solar metallicities, and a Calzetti *et al.* (2000) attenuation law, and fitted the data to obtain ages, extinctions, and metallicities. We tested how the results were affected by: (1) using Salpeter (1955), Kroupa (2001), and Chabrier (2003) IMFs; (2) different attenuation recipes, namely, Calzetti *et al.* (2000), appropriate for starburst galaxies, and the more general law from Charlot & Fall (2000); and (3) different stellar population synthesis libraries and codes, namely, BC03 using XMMILES and STELIB (Le Borgne *et al.* 2003) libraries, and MIUSCAT (Vazdekis *et al.* 2010). In all cases, we found negligible differences in the estimated ages ( $< 0.1 \text{ Gyr}$ ) and extinctions ( $0.1 \text{ mag}$ ). Our fitting method included a Montecarlo algorithm to analyze uncertainties and degeneracies (see Pérez-González *et al.* 2013). Given the short wavelength range probed by the grism data, the dust extinction was not well constrained. Indeed, we found a strong age-extinction degeneracy. For example, for the high-mass stack, equally good fits were obtained for stellar populations with relatively young ages ( $\sim 1 \text{ Gyr}$ ) and large extinctions ( $A(V) > 1.5 \text{ mag}$ ) and for older ages and lower extinctions ( $1\text{--}2 \text{ Gyr}$  and  $A(V) < 1 \text{ mag}$ ). Constraining the extinction to  $A(V) < 1 \text{ mag}$ , we found that the stacked high-mass spectrum was best fitted by a SSP with solar metallicity,  $t = 1.6 \pm 0.2 \text{ Gyr}$ , and  $A(V) = 0.5 \pm 0.3 \text{ mag}$ . The low-mass stack was best fitted with solar metallicity,  $t = 1.0 \pm 0.2 \text{ Gyr}$ , and  $A(V) = 0.7 \pm 0.3 \text{ mag}$ .

Our second age determination method used the whole UV-to-NIR stacked SED (Figures 1, 2). The SHARDS medium-band and grism data allow accurate measurements of both the  $4000 \text{ Å}$  break and the  $\text{Mg}_{\text{UV}}$  absorption, two very good age estimators (see Pérez-González *et al.* 2013; Hernán-Caballero *et al.* 2013; Ferreras *et al.* 2013b, and references therein). The wider spectral range resulted in better constraints on the age and the extinction. The best-fitting BC03/XMMILES SSP model provided  $t = 1.77 \pm 0.17 \text{ Gyr}$ ,  $A(V) = 0.60 \pm 0.06$ , and  $t = 1.02 \pm 0.15 \text{ Gyr}$  and  $A(V) = 0.70 \pm 0.06$  for the high-mass and low-mass samples, respectively (solar metallicity in both cases). Again, very similar results were obtained with other IMFs, extinction recipes, and stellar population libraries. Under an unrealistic assumption of  $A(V) = 0$ , the best-fitting ages were  $t = 1.5 \text{ Gyr}$  and  $t = 2.6 \text{ Gyr}$  for the low- and high-mass stacks, respectively. These solutions provide, based on the  $\chi^2$  values,

worse fits, and do not affect our main conclusions (cf. Section 4).

Finally, we measured the stellar population ages fitting the whole UV-to-NIR SED for each individual galaxy also using the Montecarlo method, and calculating average properties for the low and high-mass sub-samples. These were remarkably and reassuringly similar (within the uncertainties) to the ones obtained with the other methods:  $t=1.0\pm0.2$  Gyr with  $A(V)=0.9\pm0.2$  mag and  $t=1.5\pm0.3$  Gyr with  $A(V)=0.9\pm0.3$  mag for the low-mass and high-mass samples, respectively.

Our age estimations are completely consistent with those obtained by Whitaker et al. (2013) using a stacked G141 grism spectrum around the  $H\beta$  absorption also for  $UVJ$ -selected MQGs, but at  $1.4 < z < 2.2$ . They find ages between 0.9 Gyr and 1.6 Gyr for blue and red massive galaxies, very similar to the ranges we find for the our two sub-samples. Consistent ages are also found for MQGs at  $z > 1$  (selected in a variety of ways and counting with heterogeneous data) by Onodera et al. (2012), van de Sande et al. (2013), Bedregal et al. (2013), and Marchesini et al. (2014). In summary, the ages of the  $UVJ$ - and sSFR-selected  $z \sim 1$  MQGs are confidently constrained to be  $< 2$  Gyr.

### 3.2. IMF estimation

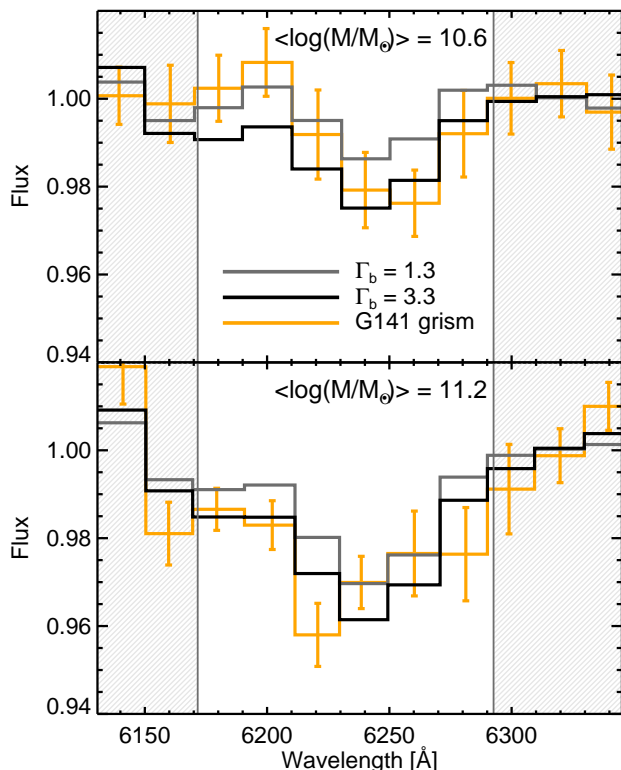


FIG. 3.— The  $\text{TiO}_2$  spectral region of the low- (top) and high-mass (bottom) stacks, as observed through the WFC3 G141 grism (orange solid line). Data points are compared to models (smoothed to the same resolution) with a bottom-heavy (black histogram) and a standard Kroupa-like IMFs (gray). The observed spectra and models were normalized to the flux in the continuum bands (gray shaded regions). Ages were fixed to the results discussed in Section 3.1.

Once average ages were determined, we proceeded to the IMF analysis based on the  $\text{TiO}_2$  absorption. Given that this molecular band dominates the spectrum of cool-dwarf stars between 600 and 640 nm, it has been widely used to infer the IMF slope in unresolved stellar systems (Ferreras et al. 2013a; La Barbera et al. 2013; Spiniello et al. 2014).

We used the MILES SSP models (Vazdekis et al. 2010), where the IMF is parametrized as a single power law, truncated (i.e., flattened out) for stellar masses below  $M < 0.6 M_\odot$ . This bimodal IMF is completely described by a single parameter,  $\Gamma_b$  (see Vazdekis et al. 1996). Under this parametrization, the Kroupa (2001) IMF is recovered for  $\Gamma_b=1.3$ . The main advantage of the bimodal IMF, compared to a regular single power law (Salpeter-like) IMF, is the fact that, even when dealing with very high  $\Gamma_b$  values, the  $M/L$  ratio remains within the observational limits suggested by dynamical studies (Ferreras et al. 2013a). From the point of view of the stellar population properties, both bimodal and uni-modal IMF parametrizations are indistinguishable.

MILES models cover a range from  $-2.32$  dex to  $+0.22$  dex in metallicity, 0.06 Gyr to 17 Gyr in age, and  $\Gamma_b=0.3$ – $3.3$  in IMF slopes. Given the weak dependence of the  $\text{TiO}_2$  index with metallicity, we fixed it to solar (as suggested by the SED fitting).

The classical definition for the  $\text{TiO}_2$  spectral index expands along  $\sim 400$  Å, making it extremely sensitive to the adopted flux calibration (see Section 5 in Martín-Navarro et al. 2014). To improve the signal, we redefined the blue and red  $\text{TiO}_2$  pseudo-continua, making them contiguous to the central bandpass. The adopted blue and red pseudo-continua are 613.0–617.2 nm and 629.3–634.5 nm, respectively. Figure 3 presents, for both stacks, the data and fits to the  $\text{TiO}_2$  spectral region.

The analysis of the  $\text{TiO}_2$  absorption was based on fits to the six spectral elements ( $P_{\text{obs}}(\lambda)$ ) within the central band of our  $\text{TiO}_2$  index definition, after removing the continuum. The models were degraded to the same spectral resolution ( $P_{\text{SSP}}(\lambda)$ ). The goodness of the fit was estimated with a  $\chi^2$  function:

$$\chi^2(\Gamma_b, \text{age}) = \sum_{\lambda} \frac{[P_{\text{obs}}(\lambda) - P_{\text{SSP}}(\lambda)]^2}{\sigma_{\text{obs}}^2(\lambda)} \quad (1)$$

where  $\sigma_{\text{obs}}(\lambda)$  represents the estimated error of the flux in each spectral bin. The  $\chi^2$  maps in the age-IMF slope plane for the low- and high-mass samples are shown in Figure 4.

## 4. DISCUSSION

Figure 4 shows our constraints on the stellar population age and IMF slope for MQGs at  $z \sim 1$ . As expected, there is a clear IMF/age degeneracy: similar  $\text{TiO}_2$  values are obtained by either an old population with a standard Kroupa-like IMF or with a steeper IMF and younger ages. To further constrain the IMF, we use the age determinations from the SED fitting.

For the high-mass sample, Figure 4 shows that our age determination of  $1.7\pm0.3$  Gyr combined with the  $\text{TiO}_2$  index measurements strongly suggest that the IMF of  $M \gtrsim 10^{11} M_\odot$  MQGs at  $z \sim 1$  is bottom-heavy. The IMF slope is  $\Gamma_b=3.2\pm0.2$ , very similar to that measured for

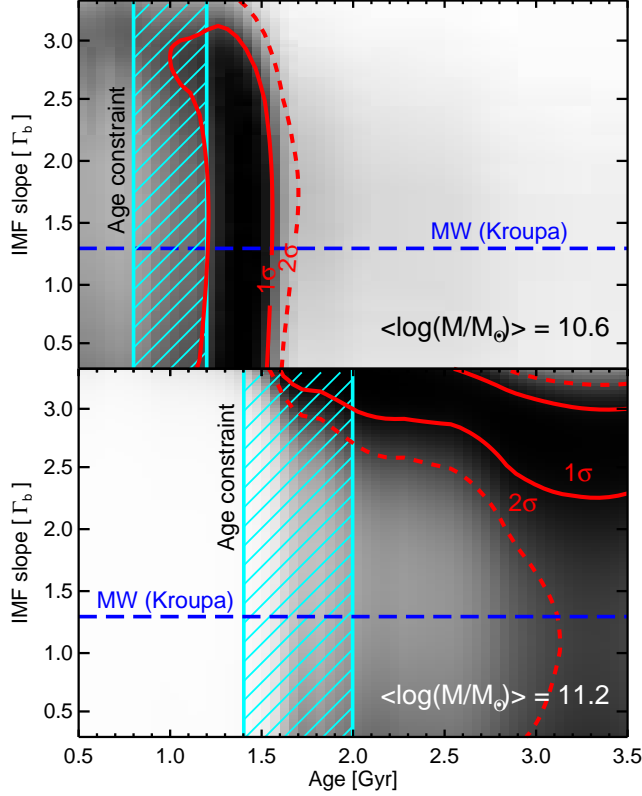


FIG. 4.—  $\chi^2$  values in the IMF slope vs. age plane for the low-mass (top) and the high-mass (bottom) samples. Darker tones indicate more probable SSP solutions. The solid and dashed red lines enclose the 1- and 2- $\sigma$  probability contours. Dashed cyan regions mark the age range inferred from SED fitting. The combination of the  $\text{TiO}_2$  index measurements and the stellar ages indicates that the IMF of massive quiescent galaxies at  $z \sim 1$  is bottom-heavy. For the low-mass galaxies, degeneracies are larger and the IMF slope determination is significantly more uncertain.

present-day early-type galaxies (La Barbera et al. 2013; Spiniello et al. 2014). For the low-mass stack, considering a typical age of  $1.0 \pm 0.2$  Gyr, we find that the IMF is flatter:  $\Gamma_b = 2.7_{-0.4}^{+0.3}$ . The uncertainty in this case is larger, mainly because the degeneracies between age and IMF increase for younger ages and flatter IMFs. Using these IMF values, and assuming a bimodal parametrization, the mass-limits of our stacks change to  $M > 10^{11.5} M_\odot$  and  $10^{10.7} < M < 10^{11.5} M_\odot$  for the high- and low-mass stacks, respectively. Although our age constraints are rather conservative (see Section 3.1), an offset of 0.5 Gyr in the lighter stack would leave the IMF slope unconstrained below  $\Gamma_b \sim 3$ . Such a large error in a 1 Gyr old population is not expected, but the IMF determination of this lighter stack should be considered more tentative than that for the massive stack. Furthermore, low-mass galaxies tend to have more extended SFHs (Thomas et al. 2005) and therefore, their SED may be less well represented by a single SSP. Note also that the departure from a SSP is expected to become larger if galaxies are observed closer to their formation age. This slightly extended star formation history in the lighter stack increases the scatter in the UV region, as shown in the upper left panel of Figures 1,2. In addition, at lower stellar masses the nature of galaxies becomes more

heterogeneous, increasing the likelihood of having systems following different evolutionary tracks (e.g., disks and spheroids with different assembly histories maybe affecting the IMF).

Two main caveats should be considered before further interpreting our data: the effect of  $\alpha$ -element enhancement and metallicity. Our fits do not account for non-solar  $\alpha$ -elements abundances. Massive galaxies exhibit an enhanced fraction of  $\alpha$ -elements compared to the solar neighborhood, commonly interpreted as an imprint of a fast formation process (Thomas et al. 2005). For a 1-2 Gyr old population, an overabundance of  $\sim 1$  dex in  $[\text{Ti}/\text{Fe}]$  would be needed to mimic the effect of a  $\Gamma_b = 3.2$  IMF (Thomas et al. 2011). However, La Barbera et al. (2013) found an excess of only  $\sim 0.2$  dex in  $[\text{Ti}/\text{Fe}]$  for massive galaxies at  $z \sim 0$ . Therefore, unless the situation is totally different at high- $z$  (but see Choi et al. 2014), our  $\text{TiO}_2$  measurement is unlikely to be explained with a standard IMF plus a non-solar  $[\text{Ti}/\text{Fe}]$  abundance. The second caveat relates to the fact that we have used models with fixed solar metallicity. The effect of the metallicity on the  $\text{TiO}_2$  line is very weak but not null. In this sense, we find steeper IMFs when assuming larger metallicities. However, neither our SED fits, nor  $z \sim 0$  massive galaxies (La Barbera et al. 2013) suggest a strong departure from solar metallicity. On the contrary, an overestimation of the actual metallicity would weakly mimic the effect of a step IMF slope on the  $\text{TiO}_2$  feature. However, sub-solar metallicities can be ruled out considering that galaxies as massive as those in our sample, show almost no metallicity evolution since  $z \sim 1$  (Choi et al. 2014), being metal-rich at  $z \sim 0$  (La Barbera et al. 2013). Thus, our results are robust against a poor metallicity determination.

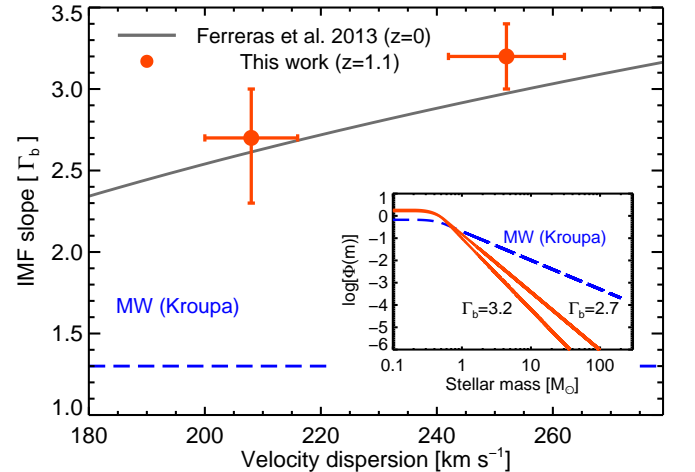


FIG. 5.— IMF slope vs. velocity dispersion for MQGs at  $z \sim 1$ , compared to the relation found for present-day ETGs (Ferreras et al. 2013a) and a Kroupa (2001) IMF. The inset explicitly shows the differences among all these IMFs.

In a more qualitative way, in Figure 5 we compare our results with the IMF slope vs. velocity dispersion relation found in the nearby Universe (Ferreras et al. 2013a). We have translated our stellar mass scale to velocity dispersion using individual measurements for our galaxies and statistical properties for samples at the same red-

shift and selected in similar way. Based on measurements found in the literature (mainly in van de Sande et al. 2013; Belli et al. 2014) for galaxies with similar masses at similar redshifts, we obtain an average velocity dispersion of  $252 \pm 10 \text{ km s}^{-1}$  and  $208 \pm 8 \text{ km s}^{-1}$  for our high- and low-mass stacks, respectively. In addition, individual velocity dispersions have been measured for two galaxies contributing to our low-mass stacked spectrum (Newman et al. 2010). The mass of one of these galaxies is  $M = 10^{10.6} M_{\odot}$  and its velocity dispersion  $\sigma = 206 \text{ km s}^{-1}$ , and for the other  $M = 10^{10.9} M_{\odot}$  and  $\sigma = 239 \text{ km s}^{-1}$ . According to Figure 5, our  $z \sim 1$  IMF estimations are in good agreement with the IMF slope in early-type galaxies of similar mass in the present-day

Universe. This suggests a direct evolutionary link between both populations and that the IMF, a key characteristic of the stellar populations in galaxies, have remained unchanged in the last  $\sim 8 \text{ Gyr}$ .

We acknowledge support from the Spanish Government grants AYA2010-21322-C03-02 and AYA2012-31277, and the ERC Advanced Grant 321323-NEOGAL. This work is based on SHARDS observations made with the Gran Telescopio Canarias (GTC), and the Rainbow Cosmological Surveys Database, operated by UCM partnered with UCO/Lick, UCSC. IMN thank Carsten Weidner, Jesús Falcón-Barroso, and Mike Beasley for their careful reading and comments on the manuscript.

#### REFERENCES

- Barro, G., Pérez-González, P. G., Gallego, J., et al. 2011a, *ApJS*, 193, 13  
—, 2011b, *ApJS*, 193, 30  
Bastian, N., Covey, K. R., & Meyer, M. R. 2010, *ARA&A*, 48, 339  
Bedregal, A. G., Scarlata, C., Henry, A. L., et al. 2013, *ApJ*, 778, 126  
Belli, S., Newman, A. B., & Ellis, R. S. 2014, *ApJ*, 783, 117  
Bruzual, G., & Charlot, S. 2003, *MNRAS*, 344, 1000  
Calzetti, D., Armus, L., Bohlin, R. C., et al. 2000, *ApJ*, 533, 682  
Cappellari, M., McDermid, R. M., Alatalo, K., et al. 2012, *Nature*, 484, 485  
Cenarro, A. J., Gorgas, J., Vazdekis, A., Cardiel, N., & Peletier, R. F. 2003, *MNRAS*, 339, L12  
Chabrier, G. 2003, *PASP*, 115, 763  
Charlot, S., & Fall, S. M. 2000, *ApJ*, 539, 718  
Choi, J., Conroy, C., Moustakas, J., et al. 2014, *ArXiv e-prints*, arXiv:1403.4932  
Conroy, C., Dutton, A. A., Graves, G. J., Mendel, J. T., & van Dokkum, P. G. 2013, *ApJ*, 776, L26  
Davé, R. 2008, *MNRAS*, 385, 147  
Ferreras, I., La Barbera, F., de la Rosa, I. G., et al. 2013a, *MNRAS*, 429, L15  
Ferreras, I., Trujillo, I., Mármol-Queraltó, E., et al. 2013b, *ArXiv e-prints*, arXiv:1312.5317  
Grogin, N. A., Kocevski, D. D., Faber, S. M., et al. 2011, *ApJS*, 197, 35  
Hernán-Caballero, A., Alonso-Herrero, A., Pérez-González, P. G., et al. 2013, *MNRAS*, 434, 2136  
Hoversten, E. A., & Glazebrook, K. 2008, *ApJ*, 675, 163  
Koekemoer, A. M., Faber, S. M., Ferguson, H. C., et al. 2011, *ApJS*, 197, 36  
Kroupa, P. 2001, *MNRAS*, 322, 231  
—, 2002, *Science*, 295, 82  
Kroupa, P., Weidner, C., Pflamm-Altenburg, J., et al. 2013, 115  
La Barbera, F., Ferreras, I., Vazdekis, A., et al. 2013, *MNRAS*, 433, 3017  
Le Borgne, J.-F., Bruzual, G., Pelló, R., et al. 2003, *A&A*, 402, 433  
Marchesini, D., Muzzin, A., Stefanon, M., et al. 2014, *ArXiv e-prints*, arXiv:1402.0003  
Martín-Navarro, I., La Barbera, F., Vazdekis, A., Falcón-Barroso, J., & Ferreras, I. 2014, *ArXiv e-prints*, arXiv:1404.6533  
Meurer, G. R., Heckman, T. M., & Calzetti, D. 1999, *ApJ*, 521, 64  
Meurer, G. R., Wong, O. I., Kim, J. H., et al. 2009, *ApJ*, 695, 765  
Mould, J. R. 1976, *A&A*, 48, 443  
Newman, A. B., Ellis, R. S., Treu, T., & Bundy, K. 2010, *ApJ*, 717, L103  
Onodera, M., Renzini, A., Carollo, M., et al. 2012, *ApJ*, 755, 26  
Pérez-González, P. G., Rieke, G. H., Villar, V., et al. 2008, *ApJ*, 675, 234  
Pérez-González, P. G., Cava, A., Barro, G., et al. 2013, *ApJ*, 762, 46  
Renzini, A. 2006, *ARA&A*, 44, 141  
Salpeter, E. E. 1955, *ApJ*, 121, 161  
Shetty, S., & Cappellari, M. 2014, *ApJ*, 786, L10  
Spiniello, C., Trager, S., Koopmans, L. V. E., & Conroy, C. 2014, *MNRAS*, 438, 1483  
Thomas, D., Maraston, C., Bender, R., & Mendes de Oliveira, C. 2005, *ApJ*, 621, 673  
Thomas, D., Maraston, C., & Johansson, J. 2011, *MNRAS*, 412, 2183  
Treu, T., Auger, M. W., Koopmans, L. V. E., et al. 2010, *ApJ*, 709, 1195  
van de Sande, J., Kriek, M., Franx, M., et al. 2013, *ApJ*, 771, 85  
van Dokkum, P. G. 2008, *ApJ*, 674, 29  
van Dokkum, P. G., & Conroy, C. 2010, *Nature*, 468, 940  
Vazdekis, A., Casuso, E., Peletier, R. F., & Beckman, J. E. 1996, *ApJS*, 106, 307  
Vazdekis, A., Sánchez-Blázquez, P., Falcón-Barroso, J., et al. 2010, *MNRAS*, 404, 1639  
Whitaker, K. E., Labbé, I., van Dokkum, P. G., et al. 2011, *ApJ*, 735, 86  
Whitaker, K. E., van Dokkum, P. G., Brammer, G., et al. 2013, *ApJ*, 770, L39